

Mitigating Trade-off: Stream and Query-guided Aggregation for Efficient and Effective 3D Occupancy Prediction

Seokha Moon^{1,3†}, Janghyun Baek¹, Giseop Kim^{2,3‡}, Jinkyu Kim¹, Sunwook Choi³

¹Korea University ²DGIST ³NAVER LABS

<https://github.com/moonseokha/StreamOcc>

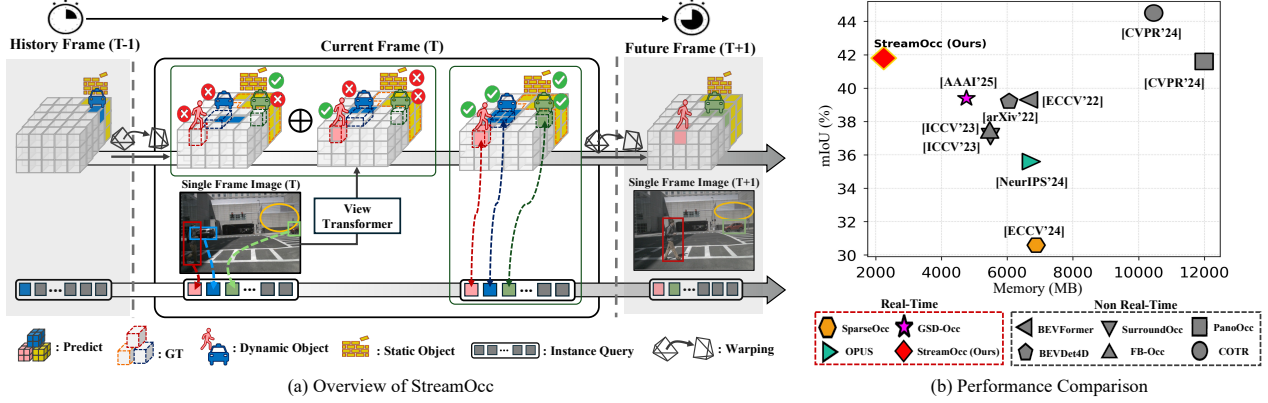


Figure 1. (a) An overview of our proposed model called *StreamOcc*, which predicts the semantic 3D occupancy states using sequentially incoming image data. Our approach accumulates voxel features in a stream-based manner while directly aggregating instance-level features of dynamic objects into corresponding voxel features, (b) showing state-of-the-art performance with higher occupancy prediction accuracy and lower computational costs, i.e., memory usage and running time. Data: Occ3D-nuScenes [21], GPU: NVIDIA A100.

Abstract

3D occupancy prediction has emerged as a key perception task for autonomous driving, as it reconstructs 3D environments to provide a comprehensive scene understanding. Recent studies focus on integrating spatiotemporal information obtained from past observations to improve prediction accuracy, using a multi-frame fusion approach that processes multiple past frames together. However, these methods struggle with a trade-off between efficiency and accuracy, which significantly limits their practicality. To mitigate this trade-off, we propose *StreamOcc*, a novel framework that aggregates spatio-temporal information in a stream-based manner. *StreamOcc* consists of two key components: (i) *Stream-based Voxel Aggregation*, which effectively accumulates past observations while minimizing computational costs, and (ii) *Query-guided Aggregation*, which recurrently aggregates instance-level features of dynamic objects into corresponding voxel features, refining fine-grained details of dynamic objects. Experiments on the Occ3D-nuScenes dataset show that *StreamOcc* achieves state-of-the-art performance in real-time settings, while reducing memory usage by more than 50% compared to previous methods.

[†]Work done during an internship at NAVER LABS.

[‡]Work done at NAVER LABS.

1. Introduction

An accurate vision-based 3D occupancy prediction, which identifies the semantic 3D occupancy states from multi-view images [21, 24, 26, 29], has become a vital perception task for autonomous vehicles to navigate dense urban areas safely. However, relying solely on single-frame and multi-view images poses challenges for accurate perception due to occlusions, which make it impossible to infer information about occluded regions, and sparsity, where 2D image features fail to project sufficient spatial information into 3D space. To address this, recent studies leverage multi-frame and multi-view images to enhance voxel representations by incorporating temporal information [6, 12, 13, 18, 20, 25]. While effective, these methods require high computational costs, including high memory usage (i.e., 5–12GB) and slow inference speed (i.e., 213–1,250ms per frame), which makes these approaches impractical for deployment in autonomous vehicles.

Towards efficient 3D occupancy prediction from multi-view and multi-frame images, several approaches have been introduced, including replacing 3D voxel representations with z-axis pooled 2D BEV representations [4, 5] and adopting sparse voxel features [16] or sparse query sets [23]. While these methods showed improved computational efficiency, their dependency on feature com-

pression or sparse sampling inevitably leads to spatial information loss, resulting in sub-optimal prediction performance. Moreover, they still need substantial memory usage ($\geq 4.8\text{GB}$) to process multi-frame inputs. Consequently, multi-frame fusion approaches still suffer from a trade-off between accuracy and efficiency, which limits their practicality for autonomous driving, where low latency, minimal memory usage, and high prediction accuracy are crucial.

Thus, in this paper, we propose a novel, efficient, yet effective 3D occupancy prediction model termed StreamOcc, which mitigates the accuracy-efficiency trade-off by applying a stream-based spatiotemporal voxel aggregation method. As shown in Figure 1 (a), our approach aligns past voxel features (containing accumulated information) with the current frame’s coordinate and integrates voxel features extracted from the current step’s multi-view images, recurrently accumulating information frame-by-frame. This method improves performance and efficiency by preserving spatial context while eliminating computational costs associated with multi-frame data processing. Maintaining temporal consistency in voxel representations, our approach effectively handles static objects, as their stationary nature prevents misalignment and facilitates precise voxel accumulation across frames. However, dynamic objects (e.g., cars, pedestrians) introduce additional challenges due to motion-induced misalignment, coarse voxel resolution (0.8m–1.6m) limiting the ability to capture small or clustered objects, and occlusions leading to incomplete depth estimation. To address these issues, we directly aggregate instance-level features, which are recurrently updated using image features that retain finer details than voxel features, into the corresponding voxel features, supplementing the information of dynamic objects that is difficult to capture solely through voxel features accumulation.

To validate our approach, we evaluate StreamOcc on the widely-used Occ3D-nuScenes [21] dataset, comparing it with other state-of-the-art approaches, including those that operate in real-time settings (i.e., $\leq 100\text{ms}$ per frame) [4, 16, 23] and non-real-time settings [6, 12, 13, 18, 25, 26].

As shown in Figure 1 (b), our model achieves matched or higher occupancy prediction performance to current SOTA approaches, requiring low computational costs, i.e., it requires approximately 2GB of memory usage and runs in 83.3ms. We summarize our contributions as follows:

- We propose a novel stream-based 3D occupancy prediction model, which effectively aggregates spatiotemporal information while running in real-time with low memory consumption and preserving dense voxel representations.
- We propose Query-guided Aggregation, which directly aggregates instance-level features of dynamic objects into voxel features, complementing fine-grained details that are difficult to capture through voxel-based accumulation.
- StreamOcc achieves state-of-the-art performance in real-

time settings on the public Occ3D-nuScenes dataset, achieving 41.90 mIoU in 83.3ms with 2,011MB of memory (less than half that of existing methods) while also supporting 3D object detection.

2. Related Work

3D Occupancy Prediction from Multi-view Images. Recent advancements in 3D occupancy prediction have focused on reconstructing complex environments, enabling a geometric and semantic understanding of the scene. Initial approaches enabled 3D occupancy prediction by transforming Bird’s Eye View (BEV) representations into dense voxel representations and incorporating segmentation heads to facilitate occupancy prediction [7, 9, 12]. To refine voxel features, SurroundOcc [26], OccFormer [29], and Occ3D [21] employed a coarse-to-fine strategy using multi-scale encoders. FB-Occ [13] further improved voxel quality by introducing a hybrid forward-backward projection that integrates depth and semantic learning. However, single-frame approaches struggle with occlusion and sparsity issues when projecting image features into 3D space. To address this, recent studies [6, 13, 18, 20, 25] have explored multi-frame fusion approach, leveraging multi past frames to enhance feature quality and scene comprehension. While processing multiple frames with dense voxel representations improves performance by preserving spatiotemporal information, it also leads to substantial memory overhead and slow inference. Consequently, these methods become impractical for deployment in autonomous vehicles with inherently limited computational resources.

Towards Efficient 3D Occupancy Prediction from Multi-frame Images. Unlike methods that maintain dense voxel representations, efficiency-driven approaches focus on reducing computational cost by leveraging sparse representations or feature compression. TPVFormer [8] employs a tri-plane structure, while FlashOcc [28] and FastOcc [5] replace 3D representations with BEV features via z-axis pooling. Moreover, GSD-Occ[4] adopts a dual-branch structure to decouple geometry and semantics for improved efficiency, SparseOcc[16] and Opus[23] utilize sparse voxel grids or sparse query sets, focusing primarily on occupied regions. However, since these methods rely on feature compression or sampling, they inherently lead to spatial information loss, and processing multiple frames still incurs high memory consumption. To address these challenges, we propose an alternative approach that achieves efficient and effective 3D occupancy prediction using a stream of sequential input images. Our approach specifically focuses on recurrently updating dense 3D voxel features at each timestep, eliminating the need for simultaneous multi-frame processing while preserving spatial information.

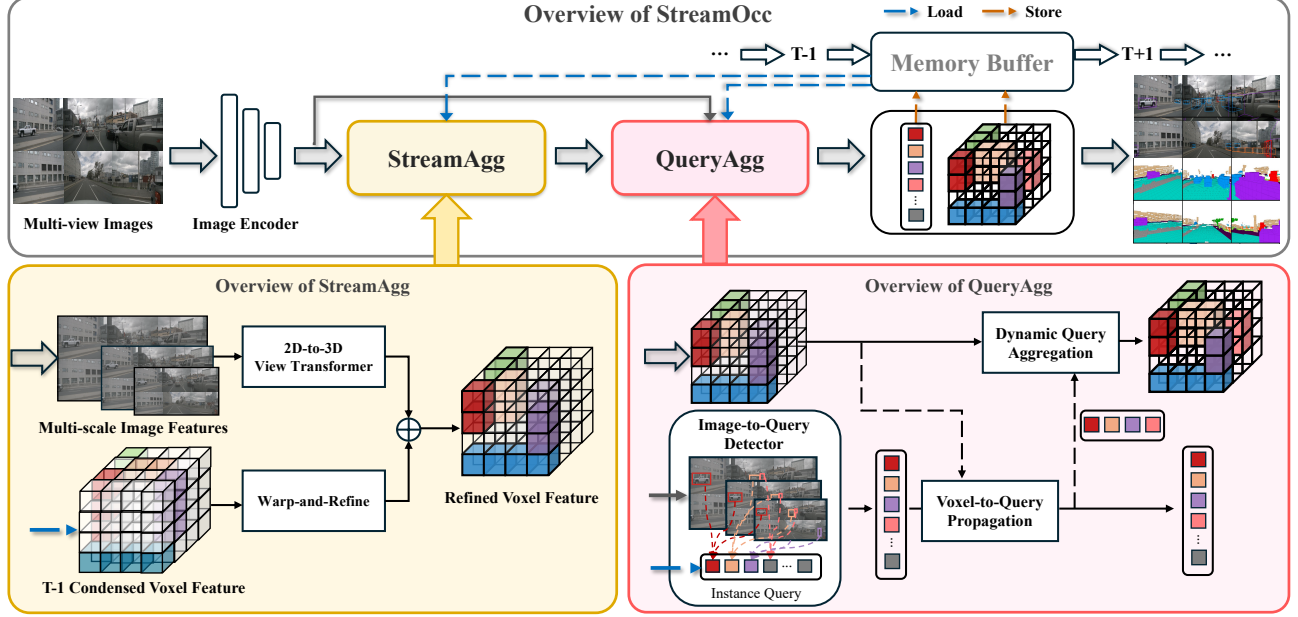


Figure 2. An overview of StreamOcc, an efficient yet effective 3D semantic occupancy prediction model that utilizes sequentially incoming multi-view images. StreamOcc comprises two key modules: (i) Stream-based Voxel Feature Aggregation (StreamAgg), which extracts voxel features at each timestep and recurrently integrates them with accumulated voxel features from past observations (Sec.3.1); and (ii) Query-guided Aggregation (QueryAgg), which recurrently updates instance queries, selects those detecting dynamic objects, and aggregates their instance-level features into corresponding voxel features to complement representations of dynamic objects (Sec. 3.2).

3. Method

In this paper, we introduce a 3D occupancy prediction called StreamOcc, a novel model designed for efficient and effective feature aggregation. As illustrated in Figure 2, StreamOcc comprises two key components: (i) Stream-based Voxel Feature Aggregation (StreamAgg) and (ii) Query-guided Aggregation (QueryAgg). The former efficiently conserves spatiotemporal information by leveraging sequentially incoming multi-view input images, where voxel features extracted from the current input are recurrently aggregated with the latest voxel features (accumulated from past observations), ensuring a seamless integration of past and present information (Sec. 3.1). Moreover, our QueryAgg enhances the representation of dynamic objects (e.g., cars and pedestrians) by selectively aggregating instance-level features from recurrently updated instance queries into their corresponding voxel features (Sec. 3.2).

3.1. Stream-based Voxel Feature Aggregation

In this section, as shown in Figure 3, we explain (i) how we extract voxel features from multi-view input images and (ii) how we recurrently aggregate them in an efficient and effective manner while preserving accumulated information from a stream of sequential inputs.

2D-to-3D View Transformation. Given a set of N_c view input images at the current timestep t , i.e., $\{\mathbf{I}_i^t\}$ for $i \in \{1, 2, \dots, N_c\}$, we follow conventions [4, 6, 18] to extract

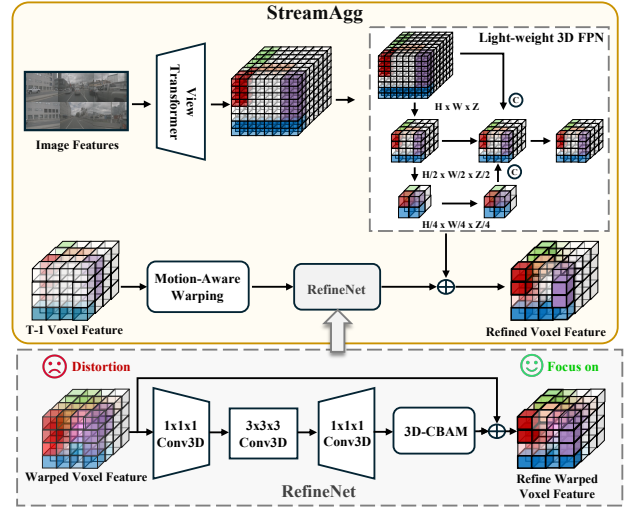


Figure 3. An overview of our Stream-based Voxel Feature Aggregation (StreamAgg) module, which recurrently aggregates 3D voxel features at every timestep in an efficient way to conserve spatiotemporal information. StreamAgg consists of three main steps: (i) 2D-to-3D view transformation, (ii) motion-aware voxel feature warping, and (iii) voxel feature refinement.

multi-scale 2D image features \mathbf{F}_i for each view image with ResNet-50 [3] and FPN [14]. Also, following the existing work [10], we apply a 2D-to-3D view transformation that projects 2D image features into a composite 3D voxel feature $\mathbf{V}_{\text{init}}^t \in \mathbb{R}^{C_{\text{init}} \times X \times Y \times Z}$. Note that X , Y , and Z denote

the voxel volume’s length, width, and height. Then, we utilize a light-weight 3D-FPN to obtain a downsampled voxel feature $\mathbf{V}^t \in \mathbb{R}^{C_v \times \frac{X}{2} \times \frac{Y}{2} \times \frac{Z}{2}}$ by subsequently aggregate multi-level voxel features. More details on Light-weight 3D-FPN are provided in the supplementary material.

Motion-aware Voxel Feature Warping. Given the 3D voxel feature \mathbf{V}^t that is produced at every timestep t and the latest accumulated voxel feature $\mathbf{V}_{\text{cond}}^{t-1} \in \mathbb{R}^{C_v \times \frac{X}{2} \times \frac{Y}{2} \times \frac{Z}{2}}$, a transformation is needed to align and aggregate them. A naive aggregation of the current and past voxel features without proper motion-aware alignment may result in spatial inconsistency. Such alignment is especially important for designing a stream-based recurrent model that only keeps a single accumulated voxel feature each time to ensure efficient computation and low memory usage. Inspired by recent work [6], we use a motion-aware voxel warping, where the spatial positions of a given voxel grid from the previous timestep $\mathbf{P}_s^e(t-1)$ are transformed into the current ego-centric coordinates with two transformation matrix, i.e., $\mathcal{T}_{e \rightarrow g}^{t-1}$ and $\mathcal{T}_{g \rightarrow e}^t$, as follows:

$$\mathbf{P}_s^e(t) = \mathcal{T}_{g \rightarrow e}^t \cdot \mathcal{T}_{e \rightarrow g}^{t-1} \cdot \mathbf{P}_s^e(t-1), \quad (1)$$

where $\mathcal{T}_{e \rightarrow g}^{t-1}$ maps ego-centric coordinates from the past timestep $t-1$ to the global coordinates, while $\mathcal{T}_{g \rightarrow e}^t$ transforms global coordinates back to the ego-centric coordinates frame at the current timestep t . The final warped voxel feature can be obtained by applying trilinear interpolation:

$$\mathbf{V}_{\text{warp}}^t = \text{Interp}(\mathbf{V}_{\text{cond}}^{t-1}, \mathbf{P}_s^e(t)), \quad (2)$$

where $\text{Interp}(\cdot)$ interpolates feature values for non-grid-aligned positions, smoothly incorporating temporal information while preserving spatial relationships.

Voxel Feature Refinement. We observe that the warped voxel features are effective and efficient in recurrently propagating spatiotemporal information. However, due to the interpolation process required in warping, these features often cause blurred object boundaries and distortions in non-occupied regions, resulting in suboptimal predictions. To mitigate this, we introduce a post-hoc refinement module called RefineNet, as illustrated in Figure 3, which enhances the warped voxel features by efficiently extracting spatial context and focusing on important regions. First, we apply a Conv3D [22] layer within a bottleneck structure [3] to the warped voxel features with reduced $C/4$ channels, enabling local context extraction at a low computational cost. Next, to assign greater importance to object-occupied regions rather than treating all voxels equally, we extend the Convolutional Block Attention Module (CBAM) [27] into 3D-CBAM. In particular, its spatial attention module leverages both average- and max-pooled features across the channel axis with a convolution kernel size of 7. This design efficiently captures a large receptive field with minimal

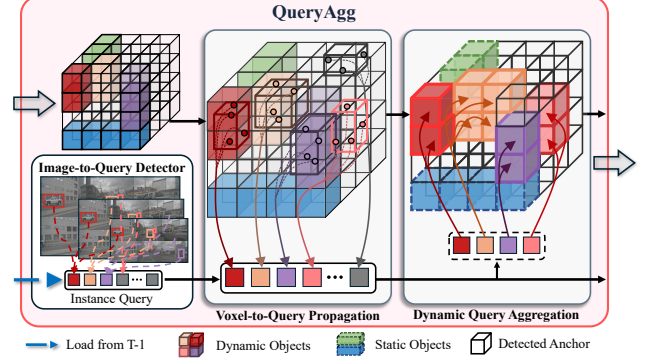


Figure 4. Overview of the Query-guided Aggregation (QueryAgg) module, which recurrently integrates instance-level features of dynamic objects into voxel features to complement fine-grained details of dynamic objects. QueryAgg consists of three steps: (i) Image-to-Query Detector, (ii) Voxel-to-Query Propagation, and (iii) Dynamic Query Aggregation.

overhead, allowing the model to better distinguish spatially important regions. Consequently, the refined spatial context selectively enhances object-relevant regions while filtering out irrelevant distortions, ensuring that the warped voxel features are effectively adjusted to capture meaningful spatial information. This refined spatial context is then fused with the original $\mathbf{V}_{\text{warp}}^t$ via a residual connection, forming the refined warped features:

$$\mathbf{V}_{\text{refwarp}}^t = \text{RefineNet}(\mathbf{V}_{\text{warp}}^t) + \mathbf{V}_{\text{warp}}^t. \quad (3)$$

This refined warped features are then merged with the current voxel features $\mathbf{V}_{\text{down}}^t$, producing:

$$\mathbf{V}_{\text{ref}} = \mathbf{V}_{\text{refwarp}}^t + \mathbf{V}_{\text{down}}^t. \quad (4)$$

3.2. Query-guided Aggregation

To complement the representation of dynamic objects (e.g., cars and pedestrians) that is difficult to capture with only accumulated voxel features, we propose Query-guided Aggregation (QueryAgg), which recurrently updates instance queries with information about dynamic objects and aggregates them into the corresponding voxel feature regions occupied by the objects. As shown in Figure 4, this module consists of the following three components: (i) Image-to-Query Detector, (ii) Voxel-to-Query Propagation, and (iii) Dynamic Query Aggregation.

Image-to-Query Detector. To precisely capture information about dynamic objects that accumulated voxel features struggle to represent, we employ an Image-to-Query Detector based on Sparse4Dv3 [15] that extracts dynamic object-specific details from 2D image features F_i and encode them into instance queries. This approach leverages the higher resolution and rich semantics of image features to enhance voxel-based representations, which struggle to effectively

capture dynamic objects. The detector applies multi-stage attention layers, where at each timestep, instance queries, initialized with anchor boxes and feature vectors, interact with multi-level image features F_i via cross-attention to refine object-specific representations. High-confidence queries are fused with those from the previous timestep to retain temporal information, while self-attention iteratively refines instance queries across timesteps, allowing recurrent updates of object-specific features. This allows instance queries to maintain temporal coherence and progressively integrate information across frames, improving representations of dynamic objects. Finally, each instance query retrieves fine-grained details from regions in F_i corresponding to predicted object locations, ensuring precise and robust dynamic object representation.

Voxel-to-Query Propagation. While instance queries from the detector provide accurate localization and retain rich semantic information about dynamic objects, they suffer from inherent uncertainty in depth estimation due to the nature of 2D monocular images. To address this, we propose Voxel-to-Query Propagation, which enhances the depth-awareness of instance queries by aggregating features from the 3D voxel grid $\mathbf{V}_{\text{ref}}^t$. Specifically, query features are refined by efficiently extracting spatial and depth information from the voxel grid using the deformable attention approach [30]. The query feature q_{vox}^i is updated as:

$$q_{\text{vox}}^i = q_{\text{img}}^i + \sum_{h=1}^H W_h \left[\sum_{o=1}^O \alpha_{iho} \cdot W_h' \cdot \mathbf{V}_{\text{ref}}^t(x_i + \Delta x_{iho}, y_i + \Delta y_{iho}, z_i + \Delta z_{iho}) \right], \quad (5)$$

where q_{img}^i is the instance feature obtained from the Image-to-Query Detector, and (x_i, y_i, z_i) denotes the query's center position. H and O represent the number of attention heads and sampling points, respectively, while α_{iho} indicates the attention weight for each sampled feature. The learnable matrices W_h and W_h' transform query and voxel features, and the offsets $(\Delta x_{iho}, \Delta y_{iho}, \Delta z_{iho})$ refine sampling positions. This refinement helps instance queries focus on informative regions, improving spatial and depth representation through fine-grained voxel feature aggregation.

Dynamic Query Aggregation. To selectively aggregate instance-level image features from instance queries that successfully detect objects into the voxel grids they occupy, we employ Dynamic Query Aggregation (DQA). DQA first filters high-confidence instance queries (i.e., those detecting dynamic objects) using a predefined threshold (detailed in the supplementary material). The selected queries are then mapped to the voxel grids occupied by the corresponding object, where query-to-voxel attention aggregates their instance features into the mapped voxel grids. This process is

formulated as:

$$\mathbf{q}^i = \mathbf{W}_Q (\mathbf{V}_{\text{ref}}^i + \sigma_p), \mathbf{k}^{ij} = \mathbf{v}^{ij} = \mathbf{W}_{K/V} q_{\text{vox}}^{ij}, \quad (6)$$

$$\alpha^i = \text{softmax} \left(\frac{(\mathbf{q}^i)^\top}{\sqrt{d}} \cdot [\mathbf{k}^{ij}]_{j \in \mathcal{N}^i} \right), \quad (7)$$

$$\mathbf{z}^i = \sum_{j \in \mathcal{N}^i} \alpha^{ij} \cdot \mathbf{v}^{ij}, \quad (8)$$

$$\mathbf{g}^i = \text{sigmoid} (\mathbf{W}^{\text{gate}} [\mathbf{V}_{\text{ref}}^i, \mathbf{z}^i]). \quad (9)$$

Here, \mathcal{N}^i represents the set of instance queries whose bounding boxes overlap with the i -th voxel grid cell, ensuring that only relevant instance queries are considered during the update. Importantly, the attention process is not applied to all voxel grid cells; instead, DQA selectively focuses on grid cells likely to contain dynamic objects, filtering out static or empty regions to reduce computational overhead. In this process, \mathbf{q}^i , \mathbf{k}^{ij} , and \mathbf{v}^{ij} are the query, key, and value features, respectively, obtained through linear projections \mathbf{W}_Q , \mathbf{W}_K , and \mathbf{W}_V . The query features \mathbf{q}^i incorporate spatial information through the positional encoding σ_p , added to the voxel feature $\mathbf{V}_{\text{ref}}^i$, which ensures that spatial relationships are explicitly encoded. The attention weights α^{ij} measure the relevance between the i -th voxel grid cell and the j -th instance query, while the aggregated features \mathbf{z}^i are adaptively modulated by a gating mechanism, parameterized by \mathbf{W}^{gate} . This gating mechanism controls the influence of \mathbf{z}^i on $\mathbf{V}_{\text{ref}}^i$, ensuring that the updated voxel grid features effectively integrate instance-level information.

For grid cells with no overlapping instance queries ($\mathcal{N}^i = \emptyset$), the original voxel feature $\mathbf{V}_{\text{ref}}^i$ remains unchanged. The updated voxel feature $\mathbf{V}_{\text{DQA}}^i$ is defined as:

$$\mathbf{V}_{\text{DQA}}^i = \begin{cases} \mathbf{V}_{\text{ref}}^i + \mathbf{g}^i \odot \mathbf{z}^i, & \text{if } \mathcal{N}^i \neq \emptyset, \\ \mathbf{V}_{\text{ref}}^i, & \text{otherwise.} \end{cases} \quad (10)$$

The updated voxel feature \mathbf{V}_{DQA} are then passed through a feed-forward network (FFN) with normalization applied before each block and residual connections, producing the final condensed voxel feature \mathbf{V}_{cond} .

3.3. Decoder for 3D Occupancy Prediction

At each timestep t , our 3D occupancy decoder outputs the current frame semantic voxel volume $\mathbf{Y}_t \in \{y_0, y_1, \dots, y_C\}^{H \times W \times Z}$ where C denotes the number of semantic classes and y_0 represents the empty voxel grid. Note that H , W , and Z denote the voxel volume's length, width, and height. Formally, from the condensed voxel feature \mathbf{V}_{cond} , we first upsample \mathbf{V}_{cond} with a factor of two via 3D deconvolution layer, producing the upsampled $\mathbf{V}_{\text{fin}} \in \mathbb{R}^{C \times X \times Y \times Z}$, each of which is then used to predict each voxels' semantics with a simple MLP-based decoder. Note that, to enhance the learning of semantic representations, we use an auxiliary mask decoder following

Table 1. **Performance comparison of 3D Occupancy Prediction methods on the Occ3D-nuScenes dataset.** Non-real-time methods are listed above and real-time methods ($\leq 100\text{ms}$) below, based on inference speed on an A100 GPU. In the real-time section, **bold** and underlined indicate the best and second-best results, respectively. (* denotes our method performing without Query-guided Aggreagation.)

Method	Venue	Backbone	Image Size	Input Type	Real-time	mIoU \uparrow	Latency (ms)	Memory (MB)
SurroundOcc [26]	ICCV'23	ResNet-101	900×1600	Single	✗	37.1	312.5	5491
FB-OCC [13]	ICCV'23	ResNet-50	256×704	Single	✗	37.5	142.8	5467
BEVFormer [12]	ECCV'22	ResNet-101	900×1600	Multi	✗	39.3	212.7	6651
BEVDet4D [6]	arXiv'22	ResNet-50	256×704	Multi	✗	39.2	1250.0	6053
PanoOcc [25]	CVPR'24	ResNet-101	864×1600	Multi	✗	41.6	333.3	11991
COTR [18]	CVPR'24	ResNet-50	256×704	Multi	✗	44.5	1111.1	10453
FastOcc [5]	ICRA'24	ResNet-101	320×800	Multi	✓	37.2	93.4	-
SparseOcc [16]	ECCV'24	ResNet-50	256×704	Multi	✓	30.9	56.5	6883
OPUS [23]	NeurIPS'24	ResNet-50	256×704	Multi	✓	35.6	75.7	6735
GSD-Occ [4]	AAAI'25	ResNet-50	256×704	Multi	✓	39.4	<u>50.0</u>	4759
StreamOcc* (Ours)	-	ResNet-50	256×704	Stream	✓	<u>40.3</u>	49.0	1829
StreamOcc (Ours)	-	ResNet-50	256×704	Stream	✓	41.9	83.3	<u>2011</u>

Co-DETR [31]. This auxiliary decoder consists of multiple heads and is built upon Mask2Former [2], a Transformer-based architecture, to predict per-class occupancy masks.

4. Experiments

4.1. Experimental Settings

Datasets. We evaluate our method on the Occ3D-nuScenes dataset [21]. This dataset consists of 700 training scenes and 150 validation scenes, with dense voxel-wise annotations covering a spatial range of $[-40\text{m}, 40\text{m}]$ in the X, Y axes and $[-1\text{m}, 5.4\text{m}]$ in the Z axis, at a voxel resolution of 0.4m^3 . Each voxel within a $200 \times 200 \times 16$ grid is classified as either occupied or not, where occupied voxels are further assigned to one of 17 semantic categories, including car, pedestrian, and bicycle.

Implementation and Evaluation Details. Following conventions [4, 6, 18, 20], we utilize ResNet-50 [3] as the image backbone, resizing the image input to (256×704) . The voxel feature \mathbf{V} generated after the view transformer, following the approach of BEVDepth [10], has a resolution of $200 \times 200 \times 16$ with 64 channels. Subsequently, the features are downsampled through a light-weight 3D-FPN, resulting in \mathbf{V}_{down} with a resolution of $100 \times 100 \times 8$ and 256 channels. For detection, a total of 900 instance queries are employed, and the Auxiliary Masked Decoder consists of 6 heads. Training is conducted for 24 epochs using AdamW [17] with a batch size of 8, gradient clipping, a learning rate of 2×10^{-4} , and a 1/3 warmup ratio over 200 iterations. FPS is measured on an A100 GPU.

Further, we assess the performance of our method using mean Intersection over Union (mIoU) to evaluate occupancy prediction, while the object detection performance of the detector utilized in the Query-guided Aggregation is measured using nuScenes Detection Score (NDS) [1] and mean Average Precision (mAP) within the same spatial range.

4.2. Experimental Results

Comparison with SOTA Approaches. In Table 1, we present a comprehensive comparison with state-of-the-art (SOTA) 3D occupancy prediction methods on the Occ3D-nuScenes dataset [21]. Note that we consider approaches that may run in real-time ($\leq 100\text{ms}$) and may not. We observe in Table 1 that our method achieves SOTA performance even without a query-guided aggregation module (QueryAgg), obtaining 40.3 mIoU with the fastest inference speed (49.0ms) and the lowest memory consumption (1,829MB). To further enhance the representation of dynamic objects, we integrate QueryAgg, which further improves the prediction performance to 41.9 mIoU while maintaining real-time capability (83.3ms, 12.0 FPS) with less than 50% of the memory usage compared to the prior most memory-efficient method, GSD-Occ [4]. We would emphasize that StreamOcc consistently outperforms existing methods that can run in real-time, achieving a +11.0 mIoU improvement over SparseOcc [16], +4.7 over FastOcc [5], +6.3 over OPUS [23], and +2.5 over GSD-Occ [4], while maintaining low latency and low memory usage. Compared to non-real-time methods, StreamOcc runs over x4.0 faster and uses x6.0 less memory than PanoOcc [25], despite achieving superior performance. While COTR [18] achieves the highest performance (44.5 mIoU), its x13.3 slower inference speed and x5.2 higher memory usage than StreamOcc, making it impractical for deployment in autonomous vehicles. These results highlight that StreamOcc mitigates the trade-off between efficiency and accuracy, achieving high 3D occupancy prediction performance while maintaining a low computational cost.

We further provide qualitative results in Figure 5, showing that our method captures more spatially detailed semantic information, effectively representing dynamic objects (Row 1, Row 2) and static objects (Row 3). Despite lower computational cost, StreamOcc maintains strong performance, highlighting its robustness and efficiency.

Table 2. **Ablation study on the Occ3D-nuScenes dataset.** Evaluates the effect of each component of StreamOcc in terms of overall mIoU (mIoU_A), dynamic and static object mIoU (mIoU_D and mIoU_S, respectively), and per-class performance.

Method	mIoU _A ↑	mIoU _D ↑	mIoU _S ↑	Dynamic Object										Static Object						others
				barrier	bicycle	bus	car	cons. veh.	motorcycle	pedestrian	traffic cone	trailer	truck	drive. surf.	other flat	sidewalk	terrain	manmade	vegetation	
GSD-Occ [4]	39.44	35.13	51.16	46.18	27.75	46.00	50.52	27.13	27.65	29.04	28.06	31.22	37.75	80.91	42.51	50.52	54.80	41.34	36.87	12.27
1 Base	36.79	32.58	48.46	44.05	22.40	44.90	49.98	21.15	23.88	25.73	25.41	32.04	36.28	78.88	41.00	48.51	51.35	38.09	32.94	8.91
2 Exp#1 + Warping	39.74	34.81	52.76	46.68	25.81	45.17	52.99	24.73	27.39	26.22	28.97	32.22	37.93	82.38	45.04	53.23	57.01	41.61	37.29	11.01
3 Exp#2 + RefineNet	40.37	35.43	53.43	47.18	26.20	45.45	53.75	24.78	29.39	26.87	29.46	32.82	38.35	83.22	45.59	53.96	57.60	42.69	37.51	11.56
4 Exp#3 + Detector	40.78	36.33	53.14	48.04	26.79	45.98	54.58	24.94	29.62	28.58	30.66	33.25	40.90	83.17	45.39	53.77	57.34	41.81	37.38	11.05
5 Exp#3 + QueryAgg (Ours)	41.90	38.12	53.31	50.81	29.62	48.54	56.10	25.43	31.36	29.97	33.02	34.59	41.87	83.33	45.90	53.79	57.30	42.33	37.22	11.14

Table 3. Effect of RefineNet components.

Method	mIoU ↑	Latency (ms)	Memory (MB)
Only Warp	39.74	43.9	1826
(+) BottleneckConv3D	40.05	44.6	1829
(+) 3D-CBAM (Ours)	40.37	49.0	1829

Table 4. Ablation Study on Image-to-Voxel Feature Aggregation

Model	mIoU ↑			Costs	
	All	Dyn.	Stat.	Latency	Mem
StreamAgg only	40.37	35.36	53.42	49.0	1829
StreamAgg + SCA	40.72	35.77	53.59	95.2	2657
StreamAgg + QueryAgg (Ours)	41.90	38.12	53.31	83.3	2011

Effect of Each Component. As shown in Table 2, we conduct an ablation study on the Occ3D-nuScenes dataset [21] to analyze each component’s impact in StreamOcc. The base model (Exp#1), which processes only single-frame data, achieves 36.79 mIoU. Exp#2 shows that Motion-Aware Warping improves performance by +2.95 (39.74), while Exp#3 mitigates warping distortions using RefineNet, increasing overall mIoU by +0.63 (40.37), dynamic object accuracy by +0.62, and static object accuracy by +0.67. Despite these gains, voxel accumulation alone struggles with dynamic object representation. To address this, Exp#4 employs a multi-head approach with an additional head for dynamic object detection, boosting dynamic accuracy. In comparison, Exp#5 (using QueryAgg), which directly aggregates dynamic object features into voxel representations, yields the most significant gain, increasing overall mIoU to 41.90 and enhancing dynamic object accuracy by +2.69 (38.12), while static object performance remains largely unchanged. Notably, these results outperform the previous SOTA method, GSD-Occ [4], across most object classes, demonstrating the effectiveness of our approach.

Effect of RefineNet Components. Table 3 shows that RefineNet effectively mitigates feature distortion in warped voxel features, improving mIoU while keeping costs low. Table 3 shows that RefineNet effectively mitigates feature distortion in warped voxel features, improving mIoU while keeping computational costs low. Each component con-

Table 5. Ablation study on Query-guided Aggregation

Model	Component			Metrics		
	I2Q	V2Q	DQA	mIoU ↑	NDS ↑	mAP ↑
A				40.37	-	-
B		✓		40.06	0.4704	0.3458
C	✓			40.42	0.4904	0.3516
D	✓	✓		40.78	0.4964	0.3620
E	✓	✓	✓	41.90	0.5001	0.3681

tributes to performance enhancement, resulting in a 0.63 mIoU increase with only a minimal cost (5.1ms and 3MB).

Effect of Query-guided Aggregation. Table 4 compares methods for aggregating image features to overcome voxel-based encoding limitations. Spatial Cross-Attention (SCA), a Transformer-based method used in prior works [18, 20, 29], distributes image features across all voxel grids, providing slight improvements. However, spatial hallucinations caused by misalignment between voxel grids and image space often causes image features to be mapped to incorrect voxels [11], along with the lack of explicit supervision in deciding what information to extract from image and where to map it, often lead to suboptimal performance. In contrast, Query-guided Aggregation (QueryAgg) explicitly extracts dynamic object features and selectively integrates them into the corresponding voxel regions. By focusing on dynamic object regions, this targeted aggregation avoids hallucinations, reduces computational overhead, and significantly improves dynamic object representation (+2.76 mIoU), achieving the superior overall performance (+1.53 over Only SVA). Despite a minor decrease in static object, the impact is negligible, and QueryAgg remains highly efficient with 83.3 ms latency and 2011 MB memory usage.

Furthermore, Figure 6 shows that QueryAgg effectively aggregates instance-level features of dynamic objects into voxel space, enhancing the representation of those that are small, distant, occluded, or closely positioned. By addressing voxel grid limitations that struggle to separate overlapping objects or capture fine details, QueryAgg enhances the overall scene understanding. Additional qualitative results can be found in the supplementary material.

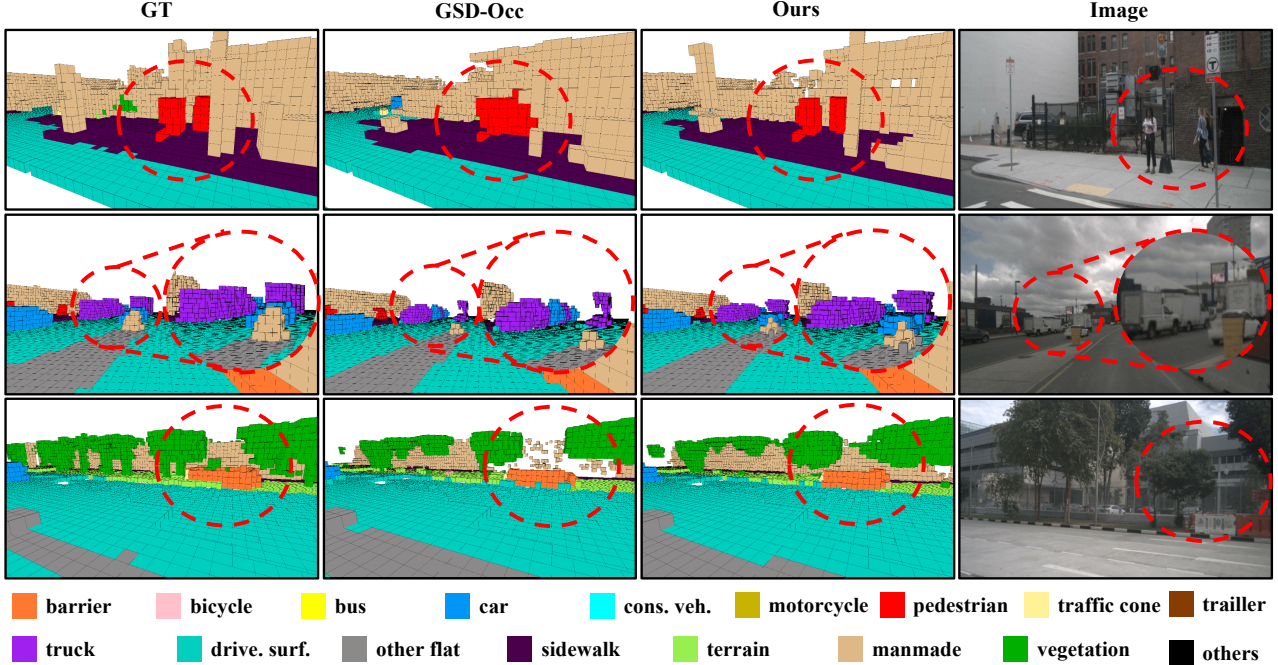


Figure 5. Visualization of qualitative results comparing GSD-Occ and our method (StreamOcc). The results demonstrate that our method captures more spatially detailed semantic information, with dynamic objects (Row 1, Row 2) and static objects (Row 3).

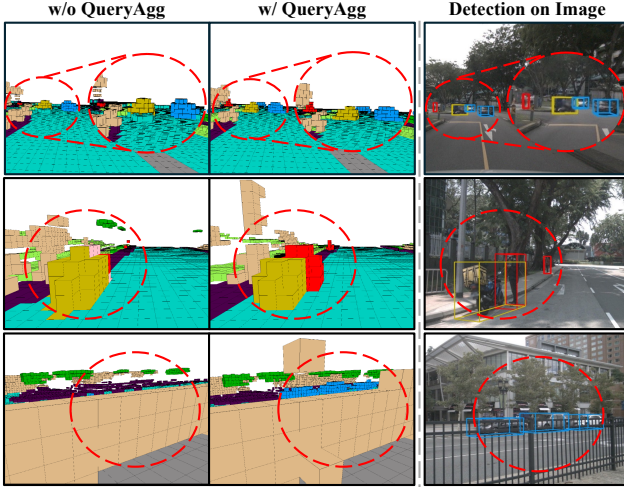


Figure 6. Visualizations of results without QueryAgg (w/o QueryAgg), with QueryAgg (w/ QueryAgg), and detection outputs from the instance queries. Red dashed circles highlight areas where QueryAgg improves the representation of dynamic objects.

How to Utilize a Detector for Joint Learning? Table 5 presents an ablation study on how detectors enhance detection and occupancy prediction. Model A serves as a baseline without a detector (StreamAgg only). Model B applies a query-based detector on voxel features for multi-task learning [19, 25], but struggles with efficiency due to the vast voxel search space and fails to detect objects missing from voxel features. Model C employs an Image-to-Query Detector [15] to enhance detection using fine-grained im-

age features but lacks direct guidance for voxel features, resulting in minimal gains. Model D refines this by first extracting semantic information about dynamic objects from images, then retrieving geometric details from depth-aware voxel features. This process provides guidance on where dynamic objects should be located within the voxel space, leading to performance improvements, though the impact remains limited. Model E (StreamOcc) aggregates instance-level features of instance queries into voxel features, enabling both to share accumulated information. This interactive framework enhances detection and occupancy prediction by leveraging distinct yet complementary features, achieving the highest NDS, mAP and mIoU.

5. Conclusion

We propose StreamOcc, a novel framework for efficient and effective 3D occupancy prediction. Our method accumulates information from sequential inputs while selectively aggregating instance-level image features to complement dynamic object representation. As a result, StreamOcc achieves SOTA performance in real-time settings while competing with SOTA non-real-time methods, all while reducing memory usage to less than 50% of existing methods on Occ3D-nuScenes. Additionally, leveraging the detector enables our model to jointly predict 3D occupancy and object poses, strengthening spatial and object-centric understanding for autonomous driving. We hope this work inspires further research into end-to-end models that integrate 3D occupancy prediction with downstream tasks.

References

- [1] Holger Caesar, Varun Bankiti, Alex H Lang, Sourabh Vora, Venice Erin Liong, Qiang Xu, Anush Krishnan, Yu Pan, Giancarlo Baldan, and Oscar Beijbom. nuscenes: A multimodal dataset for autonomous driving. In *CVPR*, pages 11621–11631, 2020. 6
- [2] Bowen Cheng, Ishan Misra, Alexander G Schwing, Alexander Kirillov, and Rohit Girdhar. Masked-attention mask transformer for universal image segmentation. In *Proceedings of the IEEE/CVF conference on computer vision and pattern recognition*, pages 1290–1299, 2022. 6, 11
- [3] Kaiming He, Xiangyu Zhang, Shaoqing Ren, and Jian Sun. Deep residual learning for image recognition. In *Proceedings of the IEEE conference on computer vision and pattern recognition*, pages 770–778, 2016. 3, 4, 6
- [4] Yulin He, Wei Chen, Tianci Xun, and Yusong Tan. Real-time 3d occupancy prediction via geometric-semantic disentanglement. *arXiv preprint arXiv:2407.13155*, 2024. 1, 2, 3, 6, 7, 11
- [5] Jiawei Hou, Xiaoyan Li, Wenhao Guan, Gang Zhang, Di Feng, Yuheng Du, Xiangyang Xue, and Jian Pu. Fastocc: Accelerating 3d occupancy prediction by fusing the 2d bird’s-eye view and perspective view. *ICRA*, 2024. 1, 2, 6
- [6] Junjie Huang and Guan Huang. Bevdet4d: Exploit temporal cues in multi-camera 3d object detection. *arXiv preprint arXiv:2203.17054*, 2022. 1, 2, 3, 4, 6
- [7] Junjie Huang, Guan Huang, Zheng Zhu, Yun Ye, and Dalong Du. Bevdet: High-performance multi-camera 3d object detection in bird-eye-view. *arXiv preprint arXiv:2112.11790*, 2021. 2
- [8] Yuanhui Huang, Wenzhao Zheng, Yunpeng Zhang, Jie Zhou, and Jiwen Lu. Tri-perspective view for vision-based 3d semantic occupancy prediction. In *Proceedings of the IEEE/CVF conference on computer vision and pattern recognition*, pages 9223–9232, 2023. 2
- [9] Yinhao Li, Han Bao, Zheng Ge, Jinrong Yang, Jianjian Sun, and Zeming Li. Bevestereo: Enhancing depth estimation in multi-view 3d object detection with temporal stereo. In *AAAI*, pages 1486–1494, 2023. 2
- [10] Yinhao Li, Zheng Ge, Guanyi Yu, Jinrong Yang, Zengran Wang, Yukang Shi, Jianjian Sun, and Zeming Li. Bevdepth: Acquisition of reliable depth for multi-view 3d object detection. In *Proceedings of the AAAI Conference on Artificial Intelligence*, pages 1477–1485, 2023. 3, 6, 11
- [11] Yiming Li, Zhiding Yu, Christopher Choy, Chaowei Xiao, Jose M Alvarez, Sanja Fidler, Chen Feng, and Anima Anandkumar. Voxformer: Sparse voxel transformer for camera-based 3d semantic scene completion. In *Proceedings of the IEEE/CVF conference on computer vision and pattern recognition*, pages 9087–9098, 2023. 7
- [12] Zhiqi Li, Wenhao Wang, Hongyang Li, Enze Xie, Chonghao Sima, Tong Lu, Yu Qiao, and Jifeng Dai. Bevformer: Learning bird’s-eye-view representation from multi-camera images via spatiotemporal transformers. In *ECCV*, pages 1–18, 2022. 1, 2, 6
- [13] Zhiqi Li, Zhiding Yu, David Austin, Mingsheng Fang, Shiyi Lan, Jan Kautz, and Jose M Alvarez. Fb-occ: 3d occupancy prediction based on forward-backward view transformation. *arXiv preprint arXiv:2307.01492*, 2023. 1, 2, 6
- [14] Tsung-Yi Lin, Piotr Dollár, Ross Girshick, Kaiming He, Bharath Hariharan, and Serge Belongie. Feature pyramid networks for object detection. In *Proceedings of the IEEE conference on computer vision and pattern recognition*, pages 2117–2125, 2017. 3
- [15] Xuewu Lin, Zixiang Pei, Tianwei Lin, Lichao Huang, and Zhizhong Su. Sparse4d v3: Advancing end-to-end 3d detection and tracking. *arXiv preprint arXiv:2311.11722*, 2023. 4, 8, 11
- [16] Haisong Liu, Haiguang Wang, Yang Chen, Zetong Yang, Jia Zeng, Li Chen, and Limin Wang. Fully sparse 3d panoptic occupancy prediction. *arXiv preprint arXiv:2312.17118*, 2023. 1, 2, 6, 11
- [17] I Loshchilov. Decoupled weight decay regularization. *arXiv preprint arXiv:1711.05101*, 2017. 6
- [18] Qihang Ma, Xin Tan, Yanyun Qu, Lizhuang Ma, Zhizhong Zhang, and Yuan Xie. Cotr: Compact occupancy transformer for vision-based 3d occupancy prediction. In *Proceedings of the IEEE/CVF Conference on Computer Vision and Pattern Recognition*, pages 19936–19945, 2024. 1, 2, 3, 6, 7
- [19] Chonghao Sima, Wenwen Tong, Tai Wang, Li Chen, Silei Wu, Hanming Deng, Yi Gu, Lewei Lu, Ping Luo, Dahua Lin, et al. Scene as occupancy. *arXiv preprint arXiv:2306.02851*, 2023. 8
- [20] Xin Tan, Wenbin Wu, Zhiwei Zhang, Chaojie Fan, Yong Peng, Zhizhong Zhang, Yuan Xie, and Lizhuang Ma. Geocc: Geometrically enhanced 3d occupancy network with implicit-explicit depth fusion and contextual self-supervision. *arXiv preprint arXiv:2405.10591*, 2024. 1, 2, 6, 7
- [21] Xiaoyu Tian, Tao Jiang, Longfei Yun, Yue Wang, Yilun Wang, and Hang Zhao. Occ3d: A large-scale 3d occupancy prediction benchmark for autonomous driving. *arXiv preprint arXiv:2304.14365*, 2023. 1, 2, 6, 7, 11
- [22] Du Tran, Lubomir Bourdev, Rob Fergus, Lorenzo Torresani, and Manohar Paluri. Learning spatiotemporal features with 3d convolutional networks. In *Proceedings of the IEEE international conference on computer vision*, pages 4489–4497, 2015. 4
- [23] Jiabao Wang, Zhaojiang Liu, Qiang Meng, Liujiang Yan, Ke Wang, Jie Yang, Wei Liu, Qibin Hou, and Mingming Cheng. Opus: occupancy prediction using a sparse set. 2024. 1, 2, 6, 11
- [24] Xiaofeng Wang, Zheng Zhu, Wenbo Xu, Yunpeng Zhang, Yi Wei, Xu Chi, Yun Ye, Dalong Du, Jiwen Lu, and Xingang Wang. Openoccupancy: A large scale benchmark for surrounding semantic occupancy perception. In *Proceedings of the IEEE/CVF International Conference on Computer Vision*, pages 17850–17859, 2023. 1
- [25] Yuqi Wang, Yuntao Chen, Xingyu Liao, Lue Fan, and Zhaoxiang Zhang. Panoocc: Unified occupancy representation for camera-based 3d panoptic segmentation. In *Proceedings of the IEEE/CVF conference on computer vision and pattern recognition*, pages 17158–17168, 2024. 1, 2, 6, 8

- [26] Yi Wei, Linqing Zhao, Wenzhao Zheng, Zheng Zhu, Jie Zhou, and Jiwen Lu. Surroundocc: Multi-camera 3d occupancy prediction for autonomous driving. In *Proceedings of the IEEE/CVF International Conference on Computer Vision*, pages 21729–21740, 2023. [1](#), [2](#), [6](#)
- [27] Sanghyun Woo, Jongchan Park, Joon-Young Lee, and In So Kweon. Cbam: Convolutional block attention module. In *Proceedings of the European conference on computer vision (ECCV)*, pages 3–19, 2018. [4](#)
- [28] Zichen Yu, Changyong Shu, Jiajun Deng, Kangjie Lu, Zong-dai Liu, Jiangyong Yu, Dawei Yang, Hui Li, and Yan Chen. Flashocc: Fast and memory-efficient occupancy prediction via channel-to-height plugin. *arXiv preprint arXiv:2311.12058*, 2023. [2](#)
- [29] Yunpeng Zhang, Zheng Zhu, and Dalong Du. Occformer: Dual-path transformer for vision-based 3d semantic occupancy prediction. In *Proceedings of the IEEE/CVF International Conference on Computer Vision*, pages 9433–9443, 2023. [1](#), [2](#), [7](#)
- [30] Xizhou Zhu, Weijie Su, Lewei Lu, Bin Li, Xiaogang Wang, and Jifeng Dai. Deformable detr: Deformable transformers for end-to-end object detection. *arXiv preprint arXiv:2010.04159*, 2020. [5](#)
- [31] Zhuofan Zong, Guanglu Song, and Yu Liu. Detrs with collaborative hybrid assignments training. In *Proceedings of the IEEE/CVF international conference on computer vision*, pages 6748–6758, 2023. [6](#)

Mitigating Trade-off: Stream and Query-guided Aggregation for Efficient and Effective 3D Occupancy Prediction

Supplementary Material

A. Further Implementation Details

Light Weight 3D-FPN. Following BEVDepth [10], we lift image features into 3D voxel features, denoted as $\mathbf{V} \in \mathbb{R}^{C \times X \times Y \times Z}$, which encode both spatial and semantic information, forming the foundation for 3D occupancy prediction. To enhance computational efficiency and capture spatial information, we apply a light weight 3D-FPN that downsamples voxel features, reducing computational costs by avoiding overly fine voxel grids.

Specifically, \mathbf{V} is passed through a Conv3D block to generate multi-scale voxel features: $\mathbf{V}_1 \in \mathbb{R}^{C_1 \times \frac{X}{2} \times \frac{Y}{2} \times \frac{Z}{2}}$ and $\mathbf{V}_2 \in \mathbb{R}^{C_2 \times \frac{X}{4} \times \frac{Y}{4} \times \frac{Z}{4}}$. These features, along with the original voxel features \mathbf{V} , are interpolated to a uniform resolution of $\frac{X}{2} \times \frac{Y}{2} \times \frac{Z}{2}$ using trilinear interpolation. The interpolated features are then concatenated and processed through a Conv1D layer to produce a compact representation $\mathbf{V}_{\text{down}} \in \mathbb{R}^{C \times \frac{X}{2} \times \frac{Y}{2} \times \frac{Z}{2}}$. By interpolating features to a lower resolution, we achieve significant computational savings while preserving spatial and semantic detail.

Query Selection for Dynamic Query Aggregation. In Dynamic Query Aggregation (DQA), the query selection process is carefully designed to avoid issues that arise when selecting queries based solely on IoU with ground-truth. This approach risks mapping all queries close to ground-truth into voxel features, regardless of whether those queries are well-detected or not. Consequently, the voxel features are trained with an implicit reliance on ground-truth information, leading to incorrect learning and overfitting.

To overcome this issue, we adopt filtering criteria during training that combine IoU with ground-truth, confidence scores, and geometric constraints to ensure reliable integration of instance-level information while maintaining model generalization. For large objects, queries are selected if they satisfy an IoU threshold of 0.4 and a confidence score above 0.3. For small objects, even slight deviations between ground-truth bounding boxes and predicted bounding boxes can result in poor IoU, making it difficult to capture queries that accurately detect small objects in 3D space. Therefore, we introduce a geometric constraint-based metric that utilizes the center point deviation D_{center} and the box size deviation D_{size} , ensuring that $(\sigma_c \cdot D_{\text{center}} + \sigma_b \cdot D_{\text{size}}) < 1.5$, where σ_c and σ_b are empirically set to 2.0 and 1.0, respectively. This approach compensates for the limitations of IoU and ensures reliable query selection for small objects in 3D space.

During inference, the filtering process is simplified to se-

lect only instance queries with a confidence score above 0.3, consistent with the detection threshold. These strategies allow DQA to integrate reliable instance-level information while enabling the model to generalize effectively while ensuring robust detection of dynamic objects.

Loss Functions. To optimize our model, we combine multiple task-specific loss functions. For depth estimation, we adopt the depth loss $\mathcal{L}_{\text{depth}}$ from BEVDepth [10]. Voxel occupancy prediction uses the cross-entropy-based occupancy loss \mathcal{L}_{occ} , applied to the predictions generated by an MLP on P_{fin} . The Image-to-Query Detector utilizes the detection loss \mathcal{L}_{det} from Sparse4D v3 [15]. To improve voxel representation, we incorporate an Auxiliary Mask Decoder with the mask loss $\mathcal{L}_{\text{mask}}$, as described in Mask2Former [2]. The total loss function $\mathcal{L}_{\text{total}}$ is defined as:

$$\mathcal{L}_{\text{total}} = \lambda_{\text{depth}} \cdot \mathcal{L}_{\text{depth}} + \lambda_{\text{occ}} \cdot \mathcal{L}_{\text{occ}} + \lambda_{\text{det}} \cdot \mathcal{L}_{\text{det}} + \lambda_{\text{mask}} \cdot \mathcal{L}_{\text{mask}}, \quad (11)$$

where λ_{depth} , λ_{occ} , λ_{det} , and λ_{mask} are the balancing weights for each loss term. In our experiments, we empirically set these weights to 0.05, 10.0, 0.2, and 1.0, respectively.

B. More Experiments

RayIoU Performance Comparison. Table 6 presents the RayIoU performance of 3D occupancy prediction methods without using the camera visibility mask for training. Our method, StreamOcc, achieves the best performance across all evaluation distances, outperforming SparseOcc by 5.9%, GSD-Occ by 2.1%, and OPUS by 0.7% in overall RayIoU. Notably, StreamOcc maintains strong long-range performance (47.1 RayIoU at 4m), demonstrating its effectiveness in capturing fine-grained spatial details. These results highlight its robustness in 3D scene understanding.

Table 6. 3D occupancy prediction performance evaluated with RayIoU, as proposed by [16], on the Occ3D-nuScenes dataset [21] without using the visibility mask during training.

Method	RayIoU	RayIoU _{1m}	RayIoU _{2m}	RayIoU _{4m}
SparseOcc [16]	35.1	29.1	35.8	40.3
GSD-Occ [4]	38.9	33.0	39.7	44.1
OPUS [23]	40.3	33.7	41.1	46.0
StreamOcc	41.1	34.2	41.9	47.1

More Visualization. Figure 7 further demonstrates the performance of StreamOcc across three distinct scenarios, comparing the ground truth, results without QueryAgg, results with QueryAgg, and detection outputs from the instance queries. The first row enhances the representation of

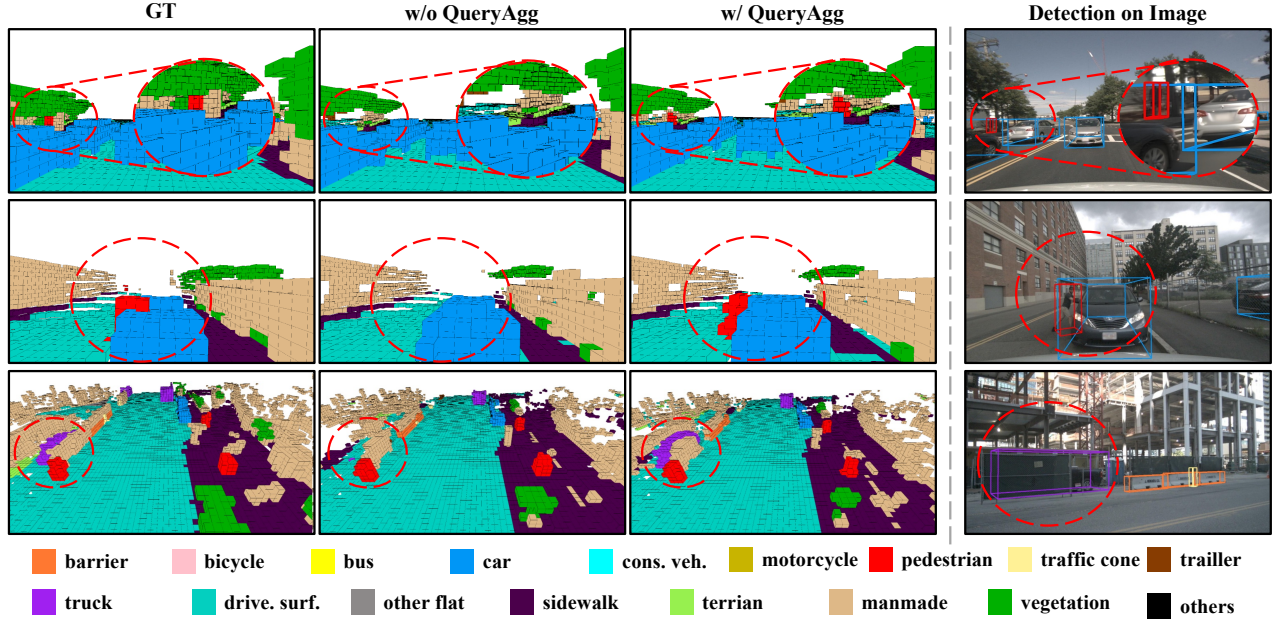


Figure 7. Visualization results of StreamOcc across three distinct scenarios. Each row shows the ground-truth (GT), results without QueryAgg (w/o QueryAgg), with QueryAgg (w/ QueryAgg), and detection outputs from the instance queries.

distant pedestrians, while the second row illustrates its ability to separate nearby objects and accurately capture their occupancy. The third row demonstrates how DQA enables the occupancy map to capture a truck that is partially obscured by a fence. Since the fence obstructs the truck in the image view, its semantic information is not well projected into the 3D space. However, by leveraging QueryAgg, the model directly aggregates object-level information, allowing the truck to be accurately represented in the occupancy map.

Additionally, Figures 8 to 11 visualize the model’s performance in complex scenarios.

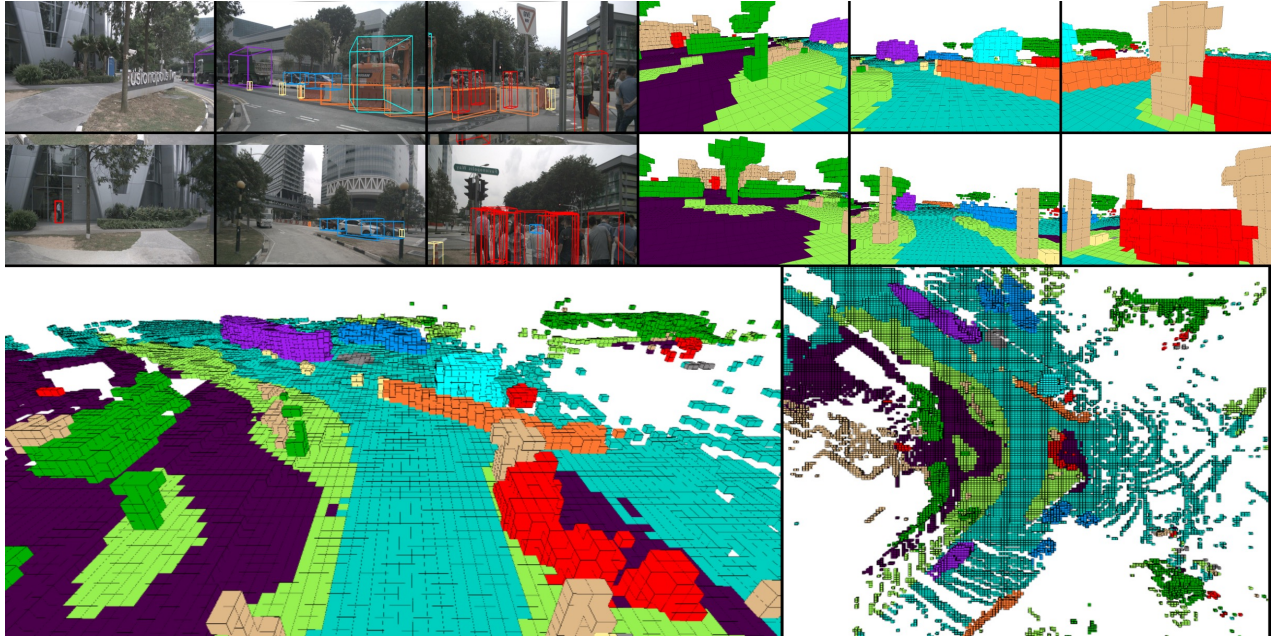


Figure 8. Visualization of 3D occupancy prediction in a dynamic urban scene with construction and pedestrians. The top-left shows object detection on the images, the top-right presents occupancy prediction in the camera view, the bottom-left illustrates the top-front view, and the bottom-right depicts the top-down occupancy prediction results.

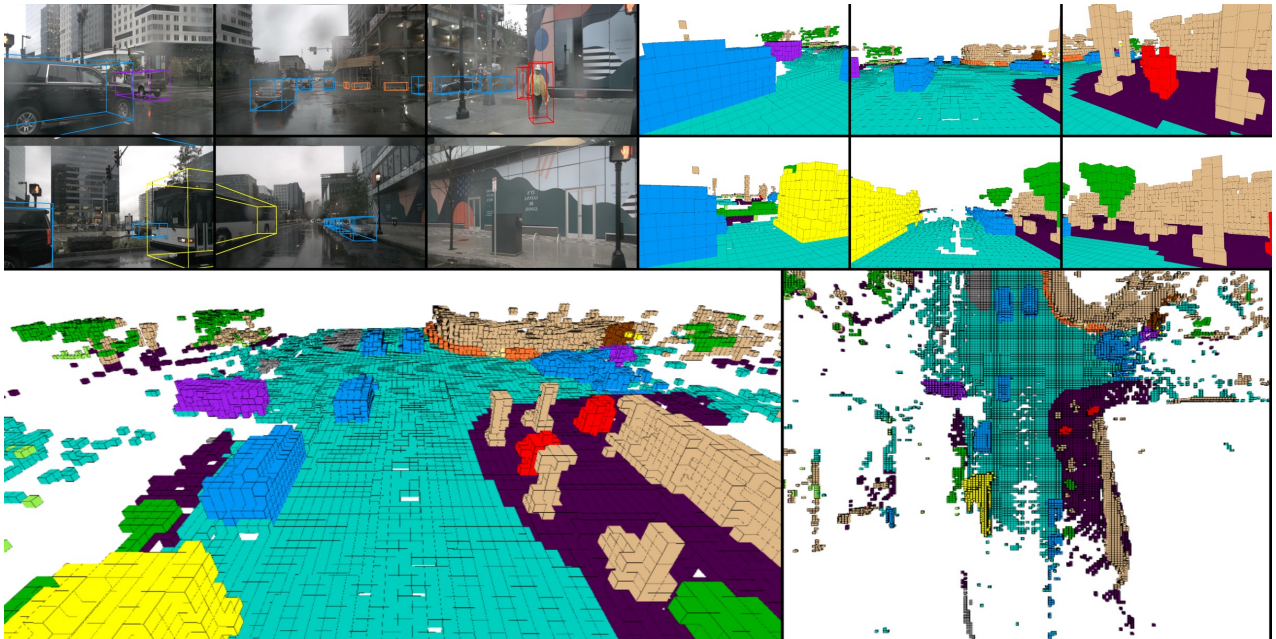
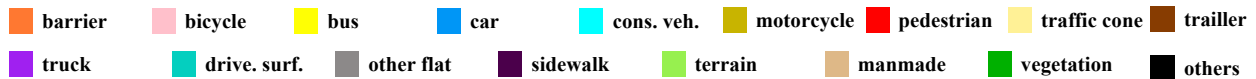


Figure 9. Visualization of 3D occupancy prediction at a crowded intersection on a rainy day. The top-left shows object detection in the image space, the top-right presents occupancy prediction in the camera view, the bottom-left illustrates the top-front view, and the bottom-right depicts the top-down occupancy prediction results.



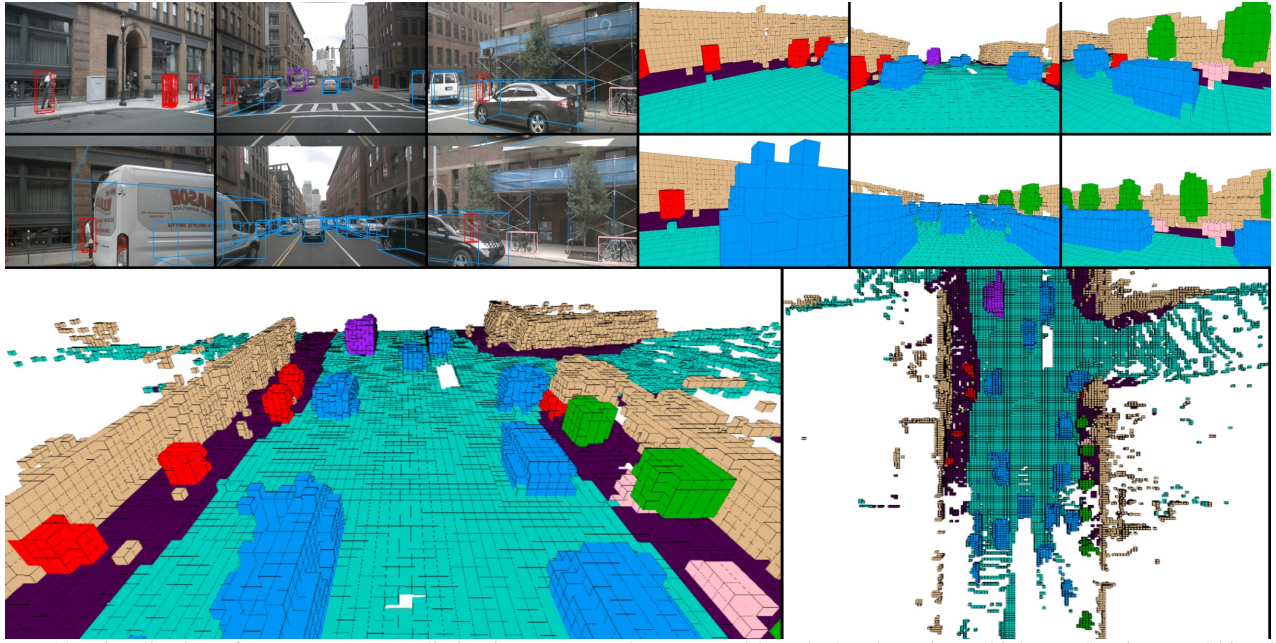


Figure 10. Visualization of 3D occupancy prediction in a narrow urban street with parked and moving vehicles, pedestrians, and bicycles. The top-left shows object detection in the image space, the top-right presents occupancy prediction in the camera view, the bottom-left illustrates the top-front view, and the bottom-right depicts the top-down occupancy prediction results.

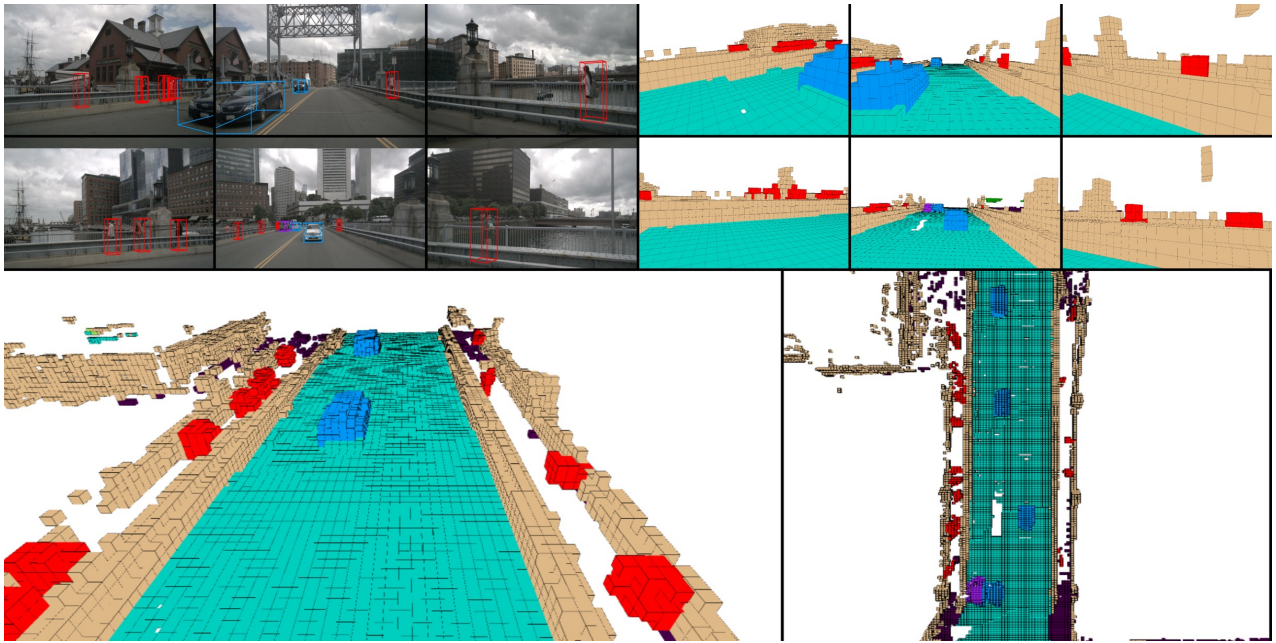


Figure 11. Visualization of 3D occupancy prediction on a bridge with moving vehicles and pedestrians. The top-left shows object detection in the image space, the top-right presents occupancy prediction in the camera view, the bottom-left illustrates the top-front view, and the bottom-right depicts the top-down occupancy prediction results.

